Chemical Tumor-Targeting of Nanoparticles Based on Metabolic Glycoengineering and Click Chemistry

Sangmin Lee,[†,‡,∥] Heebeom Koo,[†,§,∥] Jin Hee Na,[†,‡] Seung Jin Han,[†,‡] Hyun Su Min,[†] So Jin Lee,[†] Sun Hwa Kim,[†] Seok Hyun Yun,[§] Seo Young Jeong,[‡] Ick Chan Kwon,[†,⊥] Kuiwon Choi,[†,*] and Kwangmeyung Kim[†,*]

[†]Center for Theragnosis, Biomedical Research Institute, Korea Institute of Science and Technology, 39-1 Hawolgok-dong, Seongbuk-gu, Seoul 136-791, Republic of Korea., [‡]Department of Life and Nanopharmaceutical Science, Kyung Hee University, 1 Hoegi-dong, Dongdaemun-gu, Seoul 130-701, Republic of Korea, [§]Wellman Center for Photomedicine, Massachusetts General Hospital, Harvard Medical School, Cambridge, Massachusetts 02139, United States, and [⊥]KU-KIST School, Korea University, 1 Anam-dong, Seongbuk-gu, Seoul 136-701, Republic of Korea. [∥]These authors contributed equally to this work.

ABSTRACT Tumor-targeting strategies for nanoparticles have been predominantly based on optimization of physical properties or conjugation with biological ligands. However, their tumor-targeting abilities remain limited and insufficient. Furthermore, traditional biological binding molecules have intrinsic limitations originating from the limited amount of cellular receptors and the heterogeneity of tumor cells. Our two-step *in vivo* tumor-targeting strategy for nanoparticles is based on metabolic glycoengineering and click chemistry. First, an intravenous injection of precursor-loaded glycol chitosan nanoparticles generates azide groups on tumor tissue specifically by the enhanced permeation and retention (EPR) effect followed by metabolic glycoengineering. These 'receptor-like' chemical groups then enhance the tumor-targeting ability of drug-containing nanoparticles by copper-free click chemistry *in vivo* during a second intravenous injection. The advantage of this protocol over traditional binding molecules is that there are significantly more binding molecules on the surface of most tumor cells regardless of cell type. The subsequent enhanced tumor-targeting ability can significantly enhance the cancer therapeutic efficacy in animal studies.

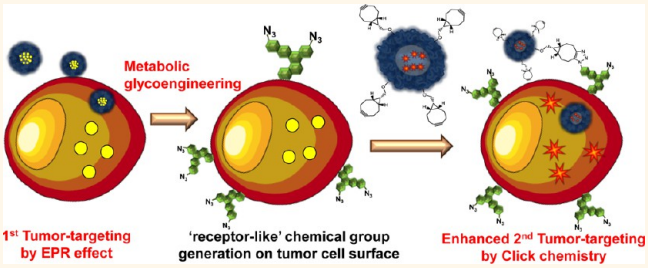

KEYWORDS: nanoparticle · click chemistry · metabolic glycoengineering · tumor-targeting · drug delivery

Click chemistry was initially named for the [3 + 2] azide−alkyne cycloaddition catalyzed by copper. Recently, this term has been broadly used for chemical reactions that have orthogonality, high yield, and a good kinetic reaction rate.[1,2] Many organic chemists have tried to remove the copper catalyst during the reaction by using cyclic ring-strain, and these trials finally resulted in 'copper-free' click chemistry several years ago.[3] Because metal catalysts like copper have severe cytotoxicity, copper-free click chemistry allows bioorthogonal chemical reactions *in vivo*.[4] A number of reports have shown broad applications of copper-free click chemistry in biological or biomedical fields such as specific labeling of proteins or nucleotides, analysis of metabolic pathways, three-dimensional assembly of cells, monitoring of zebrafish growth, and surface-modification of nanoparticles.[5−12]

Nanoparticles have been adopted in a number of biomedical applications in recent decades. Various kinds of nanoparticles have shown promising results in imaging and drug delivery for diagnostics and therapy, leading to the development of nanomedicine.[13] They can provide improved pharmacokinetics and multifunctionality compared to traditional imaging agents or drugs in the form of small molecules.[14−16] Particularly, nanoparticles exhibit relatively high accumulation in angiogenic disease sites like tumors *via* the enhanced permeation and retention (EPR) effect.[17] The tumor-targeting ability of nanoparticles can be further enhanced by physical optimization or addition of biological targeting moieties. As a result, researchers have focused on the physical properties such as the sizes and surface properties of nanoparticles suitable for EPR effect and the biological molecules (*e.g.*, antibodies, aptamers or peptides) that

* Address correspondence to kim@kist.re.kr, choi@kist.re.kr.

Received for review June 24, 2013 and accepted February 5, 2014.

Published online February 05, 2014
10.1021/nn406584y

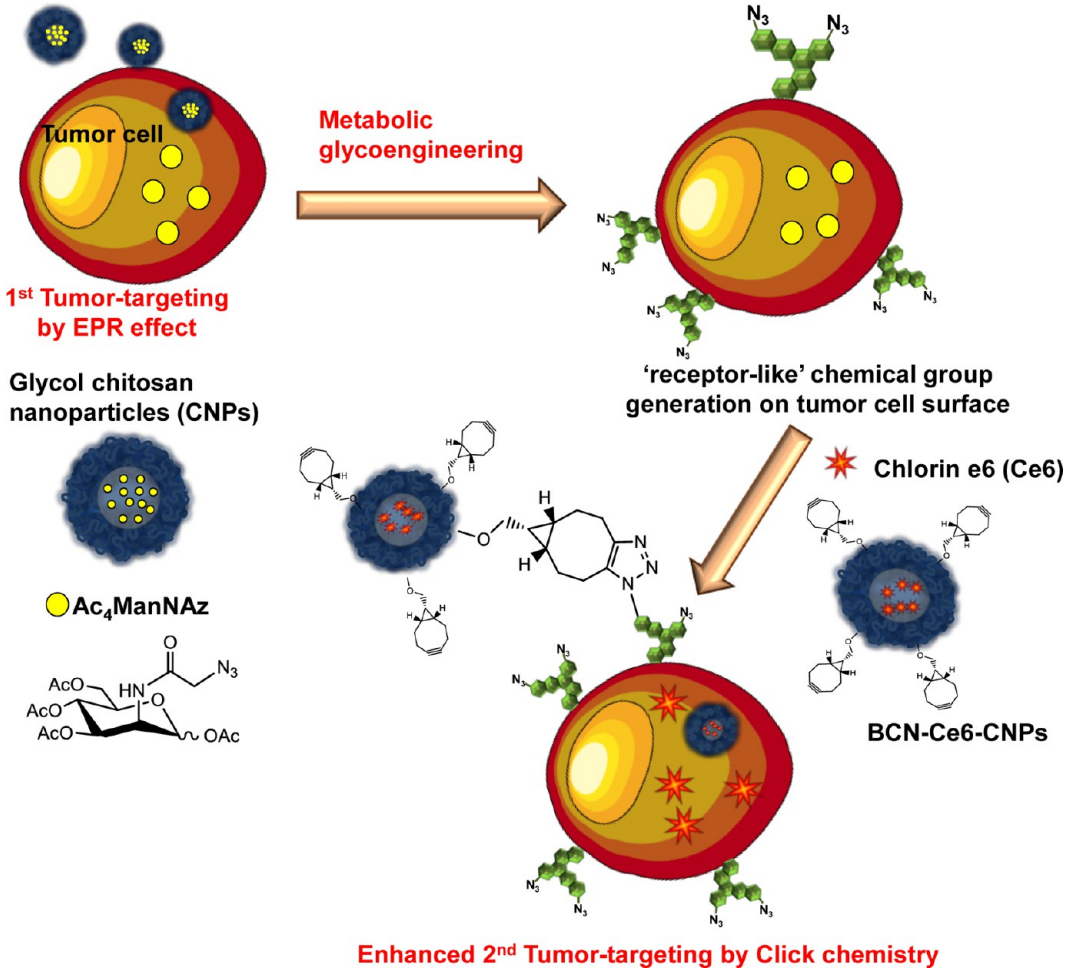

Scheme 1. Schematic illustration of the two-step *in vivo* tumor-targeting strategy for nanoparticles *via* metabolic glycoengineering and click chemistry.

enhance the binding and uptake of nanoparticles to target cells by receptor-binding.[18] However, despite the intense investigation on such methods, the tumor-targeting ability of nanoparticles is still limited and insufficient for clinical use.[19] In particular, the methods using receptor-binding molecules are intrinsically limited by the number of receptors on the tumor cell surface and the binding of nanoparticles to them can saturate.[20] In addition, the heterogeneity of tumor cells complicates the situation for various subpopulations of tumor cells expressing different types and amounts of receptors.[21]

Recently, we have shown that the biodistribution of nanoparticles after intravenous injection can be controlled by bioorthogonal copper-free click chemistry *in vivo*.[22] We used the metabolic glycoengineering technique to generate azide groups for click chemistry. Metabolic glycoengineering uses the intrinsic glycan synthesis of cells to introduce unnatural glycans with specific chemical groups by feeding the precursors used as a building block.[23] This technique has been used for the precise analysis of the cellular glycans and their metabolic pathways.[8,24] Using this technique, we can artificially generate azide groups on the tumor cells that can then be used for click chemistry *in vivo*. Even though we demonstrated that changing the pharmacokinetics of nanoparticles is feasible without biological binding molecules, precursor molecules to generate azide groups for click chemistry were delivered by intratumoral injection in that study. This intratumoral pretreatment is highly impractical from a clinical point of view because it requires the knowledge of the exact location of the tumor tissue, a case for which surgical treatment may be preferable.

Herein, we propose a two-step tumor-targeting strategy for nanoparticles using intravenous injections without any biological binding molecules. This technique can increase the tumor-targeting efficiency of nanoparticles *via* site-specific metabolic glycoengineering on tumor tissue and copper-free click chemistry *in vivo* (Scheme 1). First, tetraacetylated *N*-azidoacetyl-D-mannosamine (Ac_4ManNAz), the precursor for azide group generation, is loaded into our glycol chitosan nanoparticle (CNP) with an amphiphilic structure *via* hydrophobic interactions. Then, these Ac_4ManNAz-loaded CNPs are intravenously injected

to tumor-bearing mice. This first injection results in site-specific generation of azide groups on tumor tissue by tumor-targeted delivery of CNPs due to the EPR effect, rapid uptake of the CNP into tumor cells, and site-specific metabolic glycoengineering. In our previous papers, our CNPs showed superior tumor-targeting ability in animal models based on the EPR effect.[25,26] Their sizes are about 200 nm, but they showed long circulation in bloodstream and easily penetrated tumor vessels due to their good stability and deformability.[26] In addition, CNPs also showed reasonable uptake to tumor cells and their uptake routes were analyzed.[27] Large amount of CNPs were inside of the tumor cells within 30 min at 25 μg/mL concentration, and uptake routes included a combination of clathrin-mediated endocytosis, caveolar endocytosis, and macropinocytosis. Therefore, we expected that Ac_4ManNAz-CNPs can also deliver Ac_4ManNAz to the cytosol of tumor cells *in vivo* resulting in the generation of azide groups by metabolic engineering. Second, bicyclo[6.1.0]nonyne (BCN)-modified CNPs are intravenously injected to the same mice. Copper-free click chemistry between BCN on CNPs and azide groups on tumor tissue then results in enhanced tumor-targeting of BCN-CNP without any biological targeting moieties. When chlorine e6 (Ce6), a photosensitizer, is also conjugated onto the BCN-CNP, the enhanced tumor-targeting can increase the efficacy of photodynamic therapy *in vivo*. Importantly, this strategy is significantly different from traditional studies that simply conjugate biological molecules on nanoparticles and induce binding to intrinsic receptors on target cells. In addition, this study is also distinct from other two-step tumor-targeting studies using antibodies with avidin−biotin interaction or click chemistry because we did not use any biological targeting moieties.[28,29] Our approach generates 'receptor-like' chemical groups on the surface of target cells by nanoparticles alone, which enhances the targeting ability of drug-containing nanoparticles injected later *via* copper-free click chemistry. The advantage of this method over biological receptors is that the small azide groups can be expressed on the cell surface in large quantities regardless of the types or subpopulations of tumor cells.

RESULTS AND DISCUSSION

CNP was synthesized by conjugation of hydrophobic 5β-cholanic acid groups to the hydrophilic glycol chitosan backbone (Figure 1a).[30] This amphiphilic conjugate self-assembles into spherical nanoparticles with a diameter of about 260 nm.[31] We used Ac_4ManNAz as a precursor for azide group generation, because it can act as a building block in cell metabolism to make sialic acid, which is the most abundant glycan on the tumor cell surface (Figure 1b).[32,33] Previously, Chen group first showed that Ac_4ManNAz can be loaded to the ligand-targeted liposomes resulting in the specific metabolic glycoengineering on tumor cells at the cellular level.[34] Similarly, Ac_4ManNAz are successfully loaded into our self-assembled CNPs based on hydrophobic interactions using a traditional dialysis method.[34] The feed amount of Ac_4ManNAz was 20 wt % of CNP, and the loading efficiency of the precursor was 95.73% in the final Ac_4ManNAz-loaded CNPs (Ac_4ManNAz-CNP) (Table S1). The loading efficiency decreased to 88.26% when the feed was increased to 30 wt %, thus a 20 wt % feed of Ac_4ManNAz was maintained in the following cellular and animal studies. For the second injection, BCN was conjugated to the amine groups of CNP *via* amide bond linkages (Figure 1c and Scheme S1). BCN was selected for click chemistry *in vivo*, because it has a moderate reaction rate with azide groups, and is relatively small and less hydrophobic than DBCO that used in our previous paper.[35] In addition, Ce6, a photosensitizer, was conjugated to the second CNP instead of 5β-cholanic acid groups for photodynamic therapy of tumors.[36] About 39 molecules of Ce6 and 37 molecules of BCN were conjugated to one glycol chitosan polymer, based on ^{1}H NMR and UV−vis absorbance data after conjugation (Figure S1). The sizes and shapes of CNPs were not significantly changed after loading Ac_4ManNAz into the first CNP and conjugation of BCN and Ce6 to the second CNP design (Figure 1d,e). Their diameters of around 300 nm are suitable for blood circulation and accumulation in tumor tissue by the EPR effect.[37] After laser irradiation of the second CNP conjugated with BCN and Ce6 (BCN-Ce6-CNP), singlet oxygen was successfully generated using p-nitroso-N,N'-dimethylaniline (RNO) as an indicator (Figure S2).[38]

For *in vitro* studies, we used A549 human lung cancer cells. The goal of the *in vitro* studies was to show that similar amounts of azide groups could be generated by Ac_4ManNAz-CNP compared to free Ac_4ManNAz with the same amount of Ac_4ManNAz. It is known that the cellular uptake of free Ac_4ManNAz is very fast due to its four hydrophobic acyl groups and it generates large number of azide groups.[39] However, the situation is totally different under *in vivo* conditions, since free Ac_4ManNAz has no tumor-targeting ability *in vivo*.

First, azide group generation on the cell surface was evaluated by cellular imaging and Western blot analysis. Free Ac_4ManNAz or Ac_4ManNAz-loaded CNP was added to A549 tumor cells, and azide groups were determined by binding with DBCO-sulforhodamine B (red fluorescence).[40] After treatment of Ac_4ManNAz or Ac_4ManNAz-CNP for 3 days, the viability of A549 cells was above 90% showing no significant cytotoxicity (Figure S3). In microscopic images, the generation of azide groups was successfully observed in both free Ac_4ManNAz and Ac_4ManNAz-CNP treatment groups (Figure 2a). These images show that Ac_4ManNAz-CNP can generate azide groups on the cell surface in similar

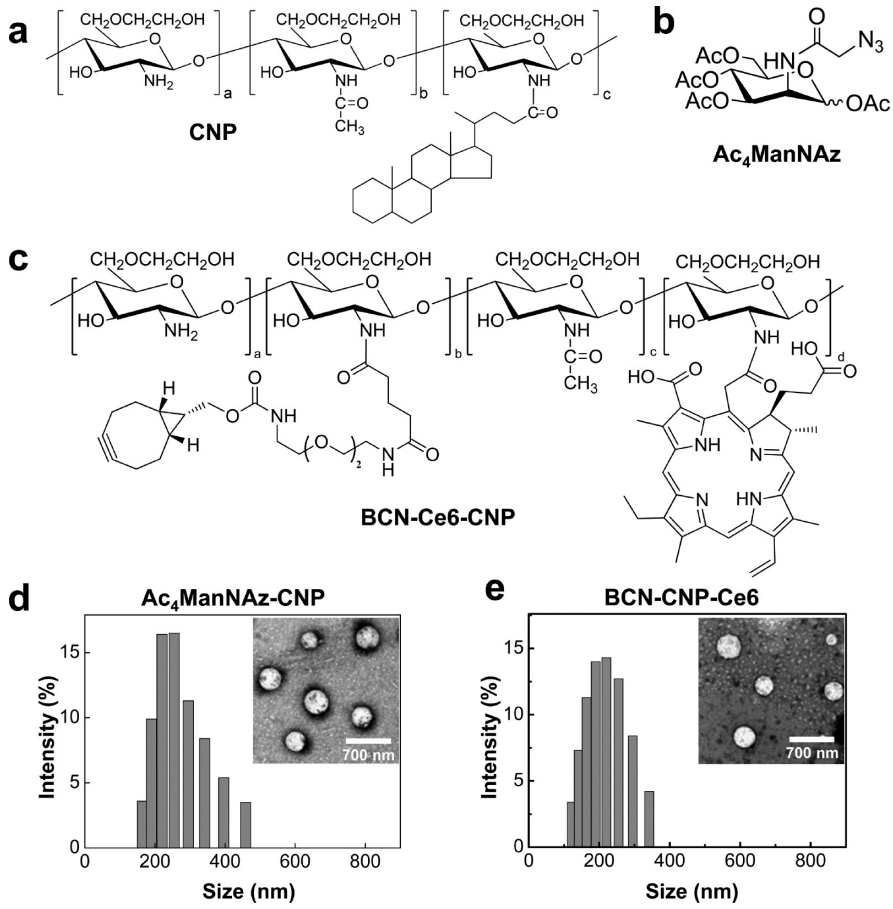

Figure 1. Physical loading of Ac_4ManNAz into glycol chitosan nanoparticle (CNP) and BCN modified second CNP containing Ce6. Chemical structures of (a) CNP, (b) Ac_4ManNAz, and (c) BCN-Ce6-CNP. Sizes and shapes of (d) Ac_4ManNAz-CNP and (e) BCN-Ce6-CNP.

quantities as free Ac_4ManNAz treatment. Western blot analysis using phosphine-PEG_3-biotin and streptavidin-HRP further demonstrated the generation of azide groups on the tumor cell surface after the treatment of free Ac_4ManNAz or Ac_4ManNAz-CNP (Figure 2b).[41] Large amounts of azide groups were generated in overall cell lysates by free Ac_4ManNAz and Ac_4ManNAz-CNP. Coomassie staining shows that the total amount of proteins was similar in all groups of cell lysates (Figure S4). The amount of azide groups on A549 cells gradually increased for 3 days during incubation with Ac_4ManNAz-CNP as shown in flow cytometry data (Figure S5). Interestingly, Ac_4ManNAz-CNP enabled longer lifetime of azide groups compared to free Ac_4ManNAz, which may be due to the sustained release of Ac_4ManNAz from the CNP and into the cytosol (Figure 2c). The longer lifetime of azide groups is another benefit of our method because it provides more time to use them. When we varied the concentration of Ac_4ManNAz-CNPs, the amounts of azide groups on the cell surface were changed (Figure 2d). This shows that our strategy can artificially introduce large number of 'receptor-like' chemical groups, overcoming the intrinsic limitations of biological targeting methods using receptor-binding molecules in which the amount of receptors on tumor cells is limited and the binding of nanoparticles to them can saturate.[20]

The heterogeneity of tumor cells complicates the situation for various subpopulations of tumor cells expressing different types and amounts of receptors.[21] This is because cancer is increasingly recognized as a combination of many disorders, each with varying causes, prognoses, and appropriate treatments. This diversity is apparent not only across different types of cancer, but also recognized within cancers of the same tissue. Furthermore, it is now known that cancer cells within the same tumor are heterogeneous in many aspects, including morphology or phenotypic expression, exhibition of inherent or acquired drug resistance, and capacity for initiating new tumor growth.[21] The heterogeneity and complexity of cancer is a big barrier of present drug delivery systems. However, our strategy can generate 'receptor-like' chemical groups on heterogeneous tumor cells by metabolic glycoengineering. To demonstrate this, we performed comparative study using representative biological ligands such as folate, cRGD, and Cetuximab (Figure 3). The biological receptors for these ligands are known to be

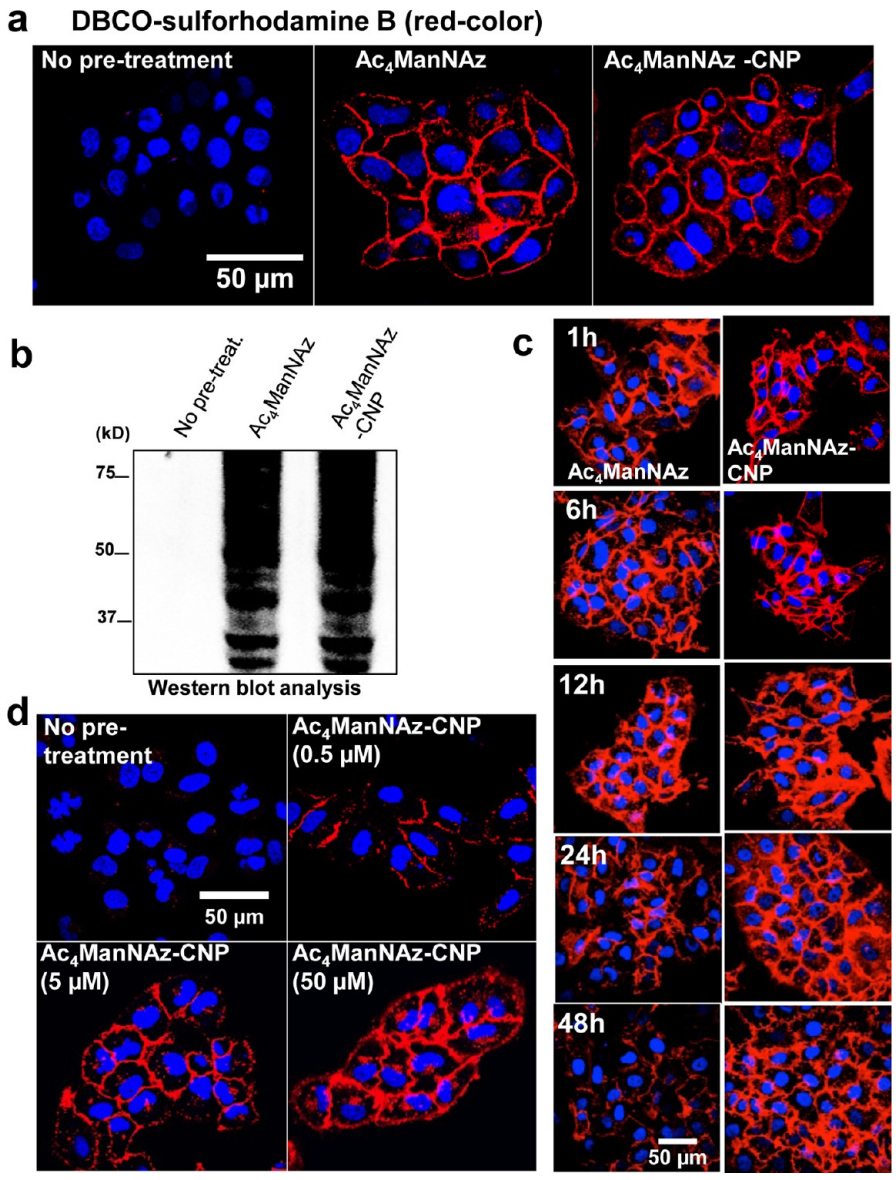

Figure 2. Azide group generation on cell surface after pretreatment of Ac_4ManNAz-CNP. (a) Visualization of azide groups on the surface of A549 tumor cells after treatment of Ac_4ManNAz-CNP. (b) Coomassie staining and Western blot analysis of cells treated with Ac_4ManNAz-CNP. (c) Time-dependent lifetime of azide groups generated by free Ac_4ManNAz (top) and Ac_4ManNAz-CNP (bottom). (d) Dose-dependent generation of azide groups on the A549 cell surface after treatment of varied concentration of Ac_4ManNAz-CNPs (0.5, 5, and 50 μM Ac_4ManNAz in media).

expressed in specific tumor cells, and each ligand labeled with dye was bound to the target cells as expected (Figure S6). However, after treatment of Ac_4ManNAz-CNPs, large amounts of azide groups were generated on all six tumor cells (KB, A549, U87MG, MCF7, MDA-MB-468, and MDA-MB-436) by metabolic glycoengineering. The azide groups were visualized by binding with dibenzylcyclooctyne-Cy5 (DBCO-Cy5), showing that they can be used for the targeting of nanoparticles containing click-chemistry molecules such as BCN or DBCO.

Next, we observed binding between the generated azide groups and BCN-Ce6-CNP. As expected, large amounts of BCN-Ce6-CNP (labeled with FITC) can bind to tumor cells pretreated with Ac_4ManNAz-CNP (Figure 4a). The fluorescence intensity of these cells was similar with the tumor cells pretreated with free Ac_4ManNAz, and higher than the control cells with no pretreatment (Figure 4b). These results demonstrate that azide groups can be generated on the tumor cell surface by Ac_4ManNAz-CNP and can increase the binding of BCN-Ce6-CNP by copper-free click chemistry. For drug delivery and tumor therapy, drug-containing nanoparticles should move into the cells after binding to the cellular membrane by click chemistry. FITC fluorescence demonstrated fast binding of BCN-Ce6-CNP to the cell membrane by click chemistry (Figure 4c). On the other hand, the intrinsic fluorescence of Ce6 was negligible initially and gradually increased with time. This increase in fluorescence is in

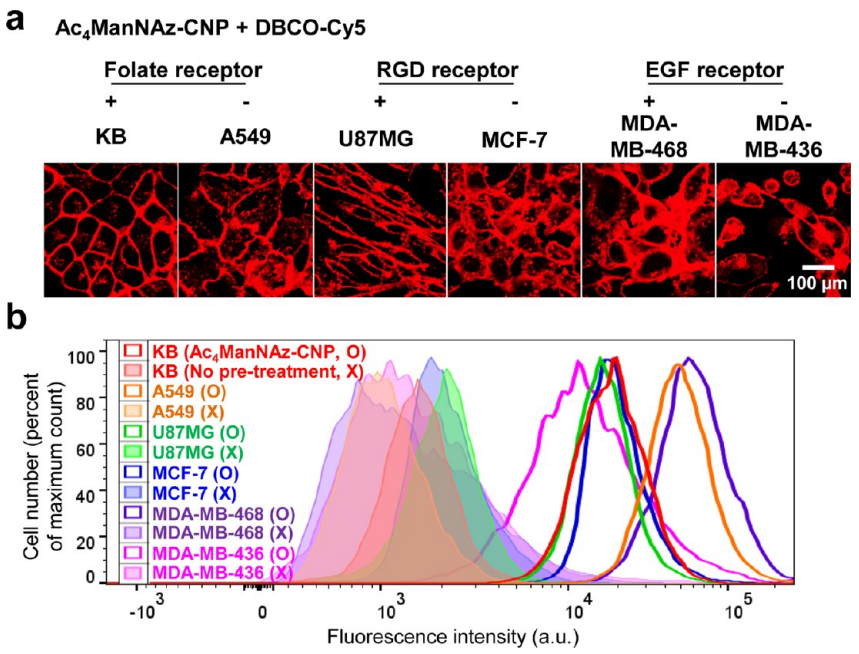

Figure 3. Generation of azide groups by Ac_4ManNAz-CNP in various tumor cells. (a) Microscopic images of tumor cells after treatment of Ac_4ManNAz-CNP and DBCO-Cy5. DBCO-Cy5 was added to tumor cells pretreated with Ac_4ManNAz-CNP (50 μM) for 3 days. (b) Flow cytometry analysis of (a).

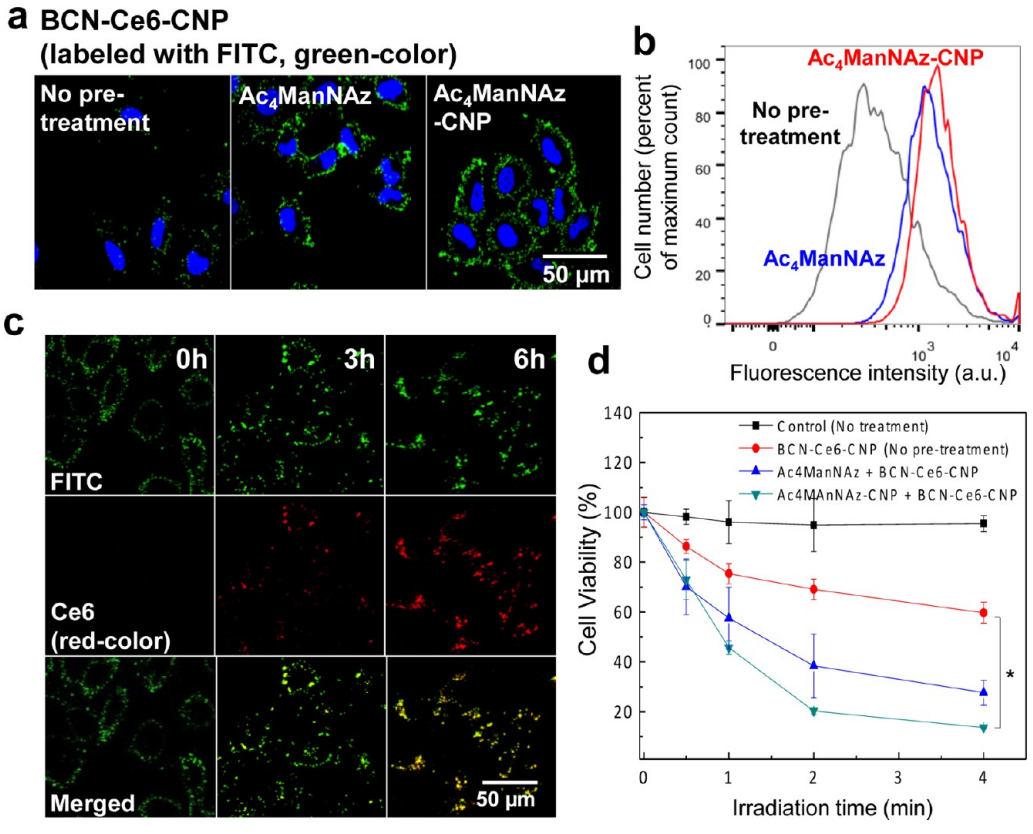

Figure 4. Cellular binding and uptake of BCN-Ce6-CNP by copper-free click chemistry. (a) Fluorescence images of cells treated with Ac_4ManNAz-CNP first and FITC-labeled BCN-Ce6-CNP second. Fluorescence signals were monitored in green channel to observe FITC-labeled CNPs (b) Flow cytometry analysis of (a). (c) Time-dependent cellular uptake of BCN-Ce6-CNP into cells pretreated with Ac_4ManNAz-CNP. (d) Viability of tumor cells treated with Ac_4ManNAz-CNP and BCN-Ce6-CNP after laser irradiation.

accordance with our previous results that reported CNPs containing photosensitizers has lower fluorescence outside of cells due to the self-quenching effect but can recover fluorescence following cellular uptake.[36]

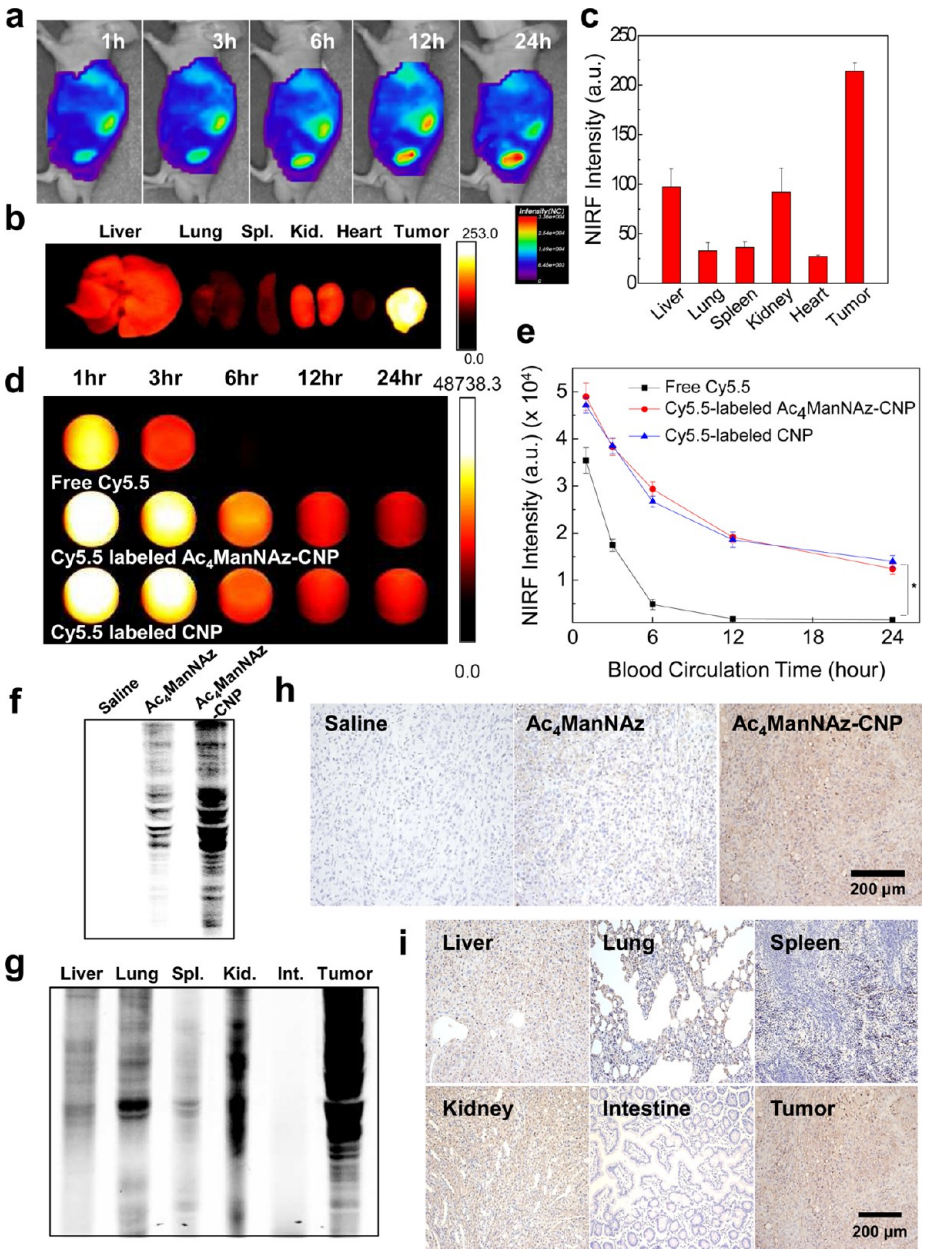

Figure 5. Intravenous injection of Ac_4ManNAz-CNP and metabolic glycoengineering on tumor tissue *in vivo*. Fluorescence signals were monitored in NIRF channel to observe Cy5.5-labeled CNPs. (a) Whole body images of mice after intravenous injection of Ac_4ManNAz-CNPs (Cy5.5-labeled). (b) *Ex vivo* fluorescence images of major organs and tumors from each group 72 h postinjection of Ac_4ManNAz-CNPs (c) Fluorescence intensities of major organs and tumor tissues from (b). (d) Fluorescence images of blood samples from the mice after intravenous injection of Cy5.5-labeled Ac_4ManNAz-CNP. (e) Fluorescence intensities of (d). Asterisk (*) indicates difference at the $p < 0.01$ significance level. ($n = 5$). (f) Western blot analysis of tumor tissues after intravenous injection of saline, free Ac_4ManNAz, or Ac_4ManNAz-CNP. (g) Western blot analysis of major organs and tumor tissue after intravenous injection of Ac_4ManNAz-CNP. (h) Histological staining of tumor tissues from (f). (i) Histological staining of major organs and tumor tissue from (g).

Cumulatively, these results indicate cellular uptake of BCN-Ce6-CNP and the possibility of intracellular drug delivery with our strategy. After laser irradiation, the viability of A549 tumor cells treated with Ac_4ManNAz-CNP and BCN-Ce6-CNP showed the fastest decrease over time among all groups as measured by an MTT assay (Figure 4d). There was negligible cell death after BCN-Ce6-CNP treatment without laser irradiation showing that the decreased viability originated from singlet oxygen generation (Figure S7). These results demonstrate that enhanced binding of drug-loaded nanoparticles by our two-step strategy can result in more effective cell killing.

The most important step of our strategy is the site-specific generation of azide groups on the tumor cell surface *in vivo* by tumor-targeted delivery of Ac_4ManNAz-CNP followed by metabolic glycoengineering. To achieve this, Ac_4ManNAz is delivered to the tumor site

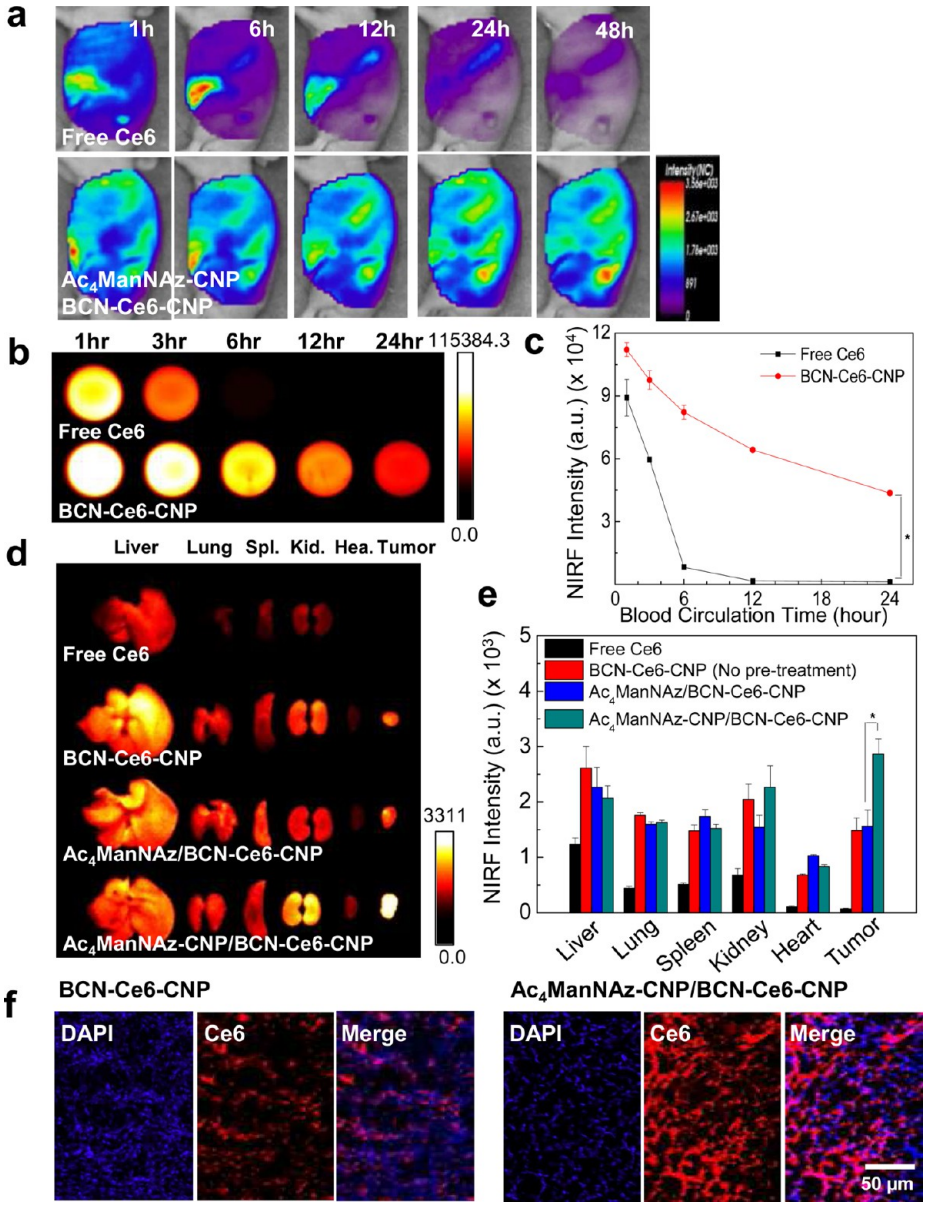

Figure 6. Biodistribution of BCN-Ce6-CNP in tumor-bearing mice after pretreatment of Ac_4ManNAz-CNP. Fluorescence signals were monitored in NIRF channel based on the intrinsic fluorescence of Ce6 in BCN-Ce6-CNP. (a) Whole body images of mice after intravenous injection of BCN-Ce6-CNP, pretreated with Ac_4ManNAz-CNP. (b) Fluorescence images of blood samples from the mice after intravenous injection of BCN-Ce6-CNP. (c) Fluorescence intensities of (b). Asterisk (*) indicates difference at the $p < 0.01$ significance level. ($n = 5$). (d) *Ex vivo* fluorescence images of major organs and tumors from each group 48 h postinjection of BCN-Ce6- CNPs. (e) Fluorescence intensities of major organs and tumor tissues from (d). (f) Fluorescence images of tumor tissues after intravenous injection of BCN-Ce6-CNP to tumor-bearing mice pretreated with saline (left panel) or Ac_4ManNAz-CNPs (right panel). Asterisk (*) indicates difference at the $p < 0.01$ significance level ($n = 3$).

by Ac_4ManNAz-CNP after intravenous injection. In previous papers, our CNPs showed superior tumor-targeting ability in animal models based on the EPR effect.[25] Various drugs including doxorubicin, paclitaxel, camptothecin, cisplatin, or photosensitizers could be delivered to the tumor site in the animal model after intravenous injection *via* the CNPs.[36,42−45] This may be based on its efficient escape from the RES in liver and long circulation time in blood flow.[26] Thus, we expected that Ac_4ManNAz can also be delivered to tumor site by Ac_4ManNAz-CNP, resulting in the azide group generation on tumor cells. In A549 tumor-bearing mice, Ac_4ManNAz-CNP labeled with Cy5.5 displayed high accumulation in tumor tissue after intravenous injection, similar to bare CNP or CNPs loaded with other chemical drugs from our previous reports (Figure 5a and Figure S8).[18,30] In the *ex vivo* analysis, tumor tissue exhibited the highest fluorescence intensity of Ac_4ManNAz-CNP compared to any other tissue type (Figure 5b,c). The NIRF (near-infrared fluorescence) images and intensity graph of blood samples obtained from tumor bearing mice after injection of particles

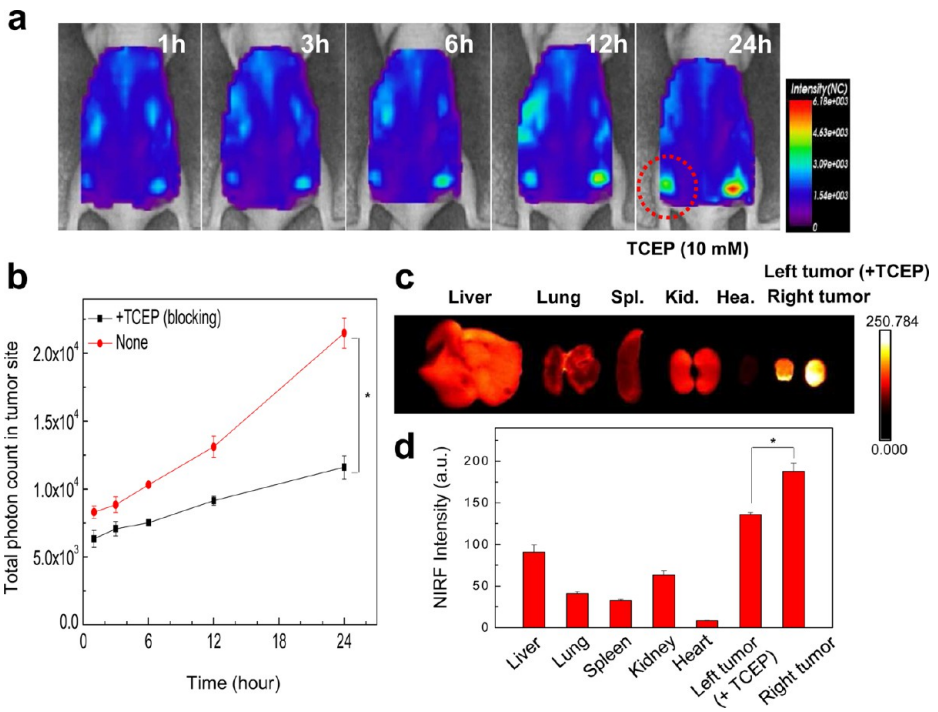

Figure 7. Biodistribution of BCN-Ce6-CNPs in mice bearing two tumors after intravenous injection of Ac_4ManNAz-CNPs, with and without TCEP treatment. Fluorescence signals were monitored in NIRF channel based on the intrinsic fluorescence of Ce6 in BCN-Ce6-CNP. (a) Whole body fluorescence images of mice after intravenous injection of BCN-Ce6-CNPs, pretreated with intravenous injection of Ac_4ManNAz-CNPs, with (left tumor) and without (right tumor) TCEP treatment. (b) Fluorescence intensities of tumor tissues from (a). (c) *Ex vivo* fluorescence images of major organs and tumors from each group 24 h postinjection of BCN-Ce6-CNPs. (d) Fluorescence intensities of major organs and tumor tissues from (c). Asterisk (*) indicates difference at the $p < 0.01$ significance level ($n = 3$).

also showed much longer circulation time of Ac_4ManNAz-CNPs than free Cy5.5 in blood flow (Figure 5d,e). This indicates that Ac_4ManNAz-CNPs have longer blood circulation times than smaller dyes, rendering them is suitable for tumor accumulation *via* the EPR effect. Azide groups generated on tumor tissue were determined by Western blot analysis and histochemical staining. After intravenous injection of saline, free Ac_4ManNAz, and Ac_4ManNAz-CNP, the major organs and tumors were collected and analyzed. Compared to saline and free Ac_4ManNAz, the tumor tissue from mice injected with Ac_4ManNAz-CNP revealed a strong band in Western blot analysis (Figure 5f). The image shows that a large number of azide groups were generated on tumor tissue by Ac_4ManNAz-CNP and metabolic glycoengineering. Importantly, the band intensity of tumor tissue was higher than those of any other organ, demonstrating the main advantage of using CNPs for tumor-targeted delivery of Ac_4ManNAz (Figure 5g). The azide groups can be specifically generated in tumor tissue by Ac_4ManNAz-CNP because of its tumor-targeting ability *via* the EPR effect. On the other hand, the intravenous injection of Ac_4ManNAz results in the generation of azide groups mainly in the liver and kidney even though the number of azide groups generated by Ac_4ManNAz and Ac_4ManNAz-CNP were similar *in vitro* (Figure S9). This is because that free Ac_4ManNAz has no tumor-targeting ability *in vivo*.

Immunohistological staining also showed enhanced generation of azide groups in tumor tissue of mice injected with Ac_4ManNAz-CNP when compared to injection of free Ac_4ManNAz (Figure 5h). Compared to other organs, the dark brown spots were more intense in tumor tissue after injection of Ac_4ManNAz-CNP (Figure 5i). These results demonstrate that metabolic glycoengineering can specifically occur on the tumor tissue after intravenous injection of Ac_4ManNAz-CNP. A large number of azide groups can be successfully generated on tumor tissue *in vivo*.

Encouraged by these results, we used azide groups generated on tumor tissue for the tumor-targeted delivery of second CNPs by copper-free click chemistry. BCN-Ce6-CNPs were intravenously injected into tumor-bearing mice which were pretreated with either saline, free Ac_4ManNAz, or Ac_4ManNAz-CNP (Figure S10). Then, the biodistribution of BCN-Ce6-CNPs were analyzed by time-dependent whole body imaging and *ex vivo* fluorescence analysis.[46] Over time, intense fluorescence signals of the second CNP emerged in tumor tissue of all groups compared to free Ce6, since CNPs have a tumor-targeting ability based on the EPR effect (Figure 6a and Figure S11). The longer circulation time of BCN-Ce6-CNPs compared to free Ce6 is also explained by the EPR effect of CNPs (Figure 6b and 6c). The signal intensity in tumor tissue was about 1.8-fold higher in the mice pretreated with Ac_4ManNAz-CNP

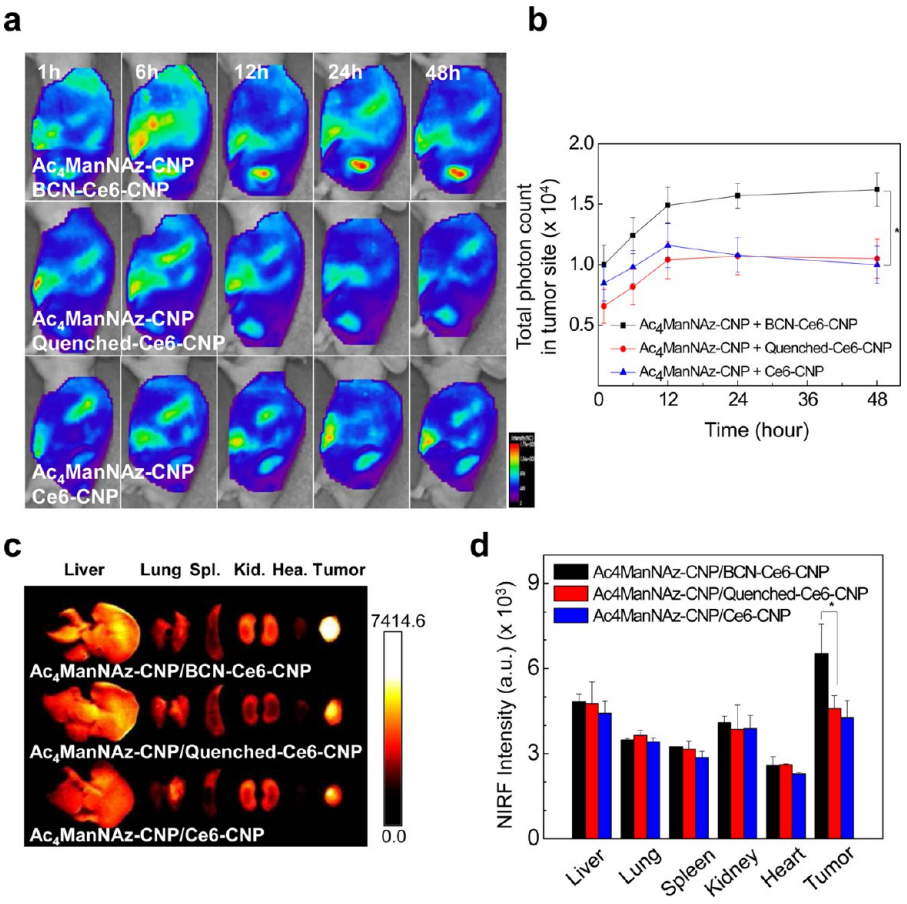

Figure 8. *In vivo* **biodistribution of quenched-Ce6-CNP in tumor-bearing mice after pretreatment of Ac_4ManNAz-CNP. Fluorescence signals were monitored in NIRF channel based on the intrinsic fluorescence of Ce6 in BCN-Ce6-CNP. (a) Whole body images of mice after intravenous injection of quenched-Ce6-CNP, pretreated with Ac_4ManNAz-CNP. (b) Fluorescence intensities in tumor site from (a). (c)** *Ex vivo* **fluorescence images of major organs and tumors from each group 48 h postinjection of quenched-Ce6-CNP. (d) Fluorescence intensities of major organs and tumor tissues from (b). Asterisk (*) indicates difference at the $p < 0.01$ significance level. ($n = 3$).**

than the saline or free Ac_4ManNAz pretreated groups and more than 10-fold higher than free Ce6 treatment. This indicates that more CNPs accumulated in the tumor region after azide generation. After 48 h, the mice were sacrificed for *ex vivo* analysis of major organs and tumors. In *ex vivo* fluorescence images, the tumor tissue from mice pretreated with Ac_4ManNAz-CNP was significantly brighter than any other organ or tumor tissue after saline or free Ac_4ManNAz pretreatment (Figure 6d). The fluorescence intensity of tumor tissue from mice pretreated with Ac_4ManNAz-CNP was also about 2-fold higher than groups pretreated with saline or free Ac_4ManNAz (Figure 6e,f). For precise analysis of this enhanced tumor-targeted delivery of the second CNPs, we designed a mice model bearing two A549 tumors on the back of each mouse and Ac_4ManNAz-CNP was injected into these mice intravenously. Then, we treated left tumors by direct injection of tris(2-carboxyethyl)-phosphine (TCEP) for chemical quenching of azide groups.[10] After intravenous injection of BCN-Ce6-CNP, the time-dependent fluorescence changes in the tumor site were significantly different between the left and right tumors (Figure 7a). As shown in both *in vivo* and *ex vivo* analysis, the accumulation of BCN-Ce6-CNP decreased by about half in the case of TCEP-injected left tumors (Figure 7b–d). This result signifies that chemical binding between BCN and azide groups is responsible for the increased accumulation of BCN-Ce6-CNPs in tumor tissue of mice pretreated with Ac_4ManNAz-CNP. To further demonstrate the pivotal role of click chemistry *in vivo* for enhanced tumor accumulation, we synthesized quenched-Ce6-CNP by treating azido acetic acid to BCN-Ce6-CNP. This control nanoparticle has no reactivity to azide groups. After intravenous injection to tumor-bearing mice, quenched-Ce6-CNP showed similar biodistribution with Ce6-CNP and their tumor accumulation. However, BCN-Ce6-CNP showed about 1.5-fold increased tumor accumulation compared to quenched-Ce6-CNP and Ce6-CNP (Figure 8). Cumulatively, these results demonstrate that more BCN-Ce6-CNP can be delivered to tumor tissue after intravenous injection using copper-free click chemistry with azide groups, which were generated by the first injection of Ac_4ManNAz-CNP.

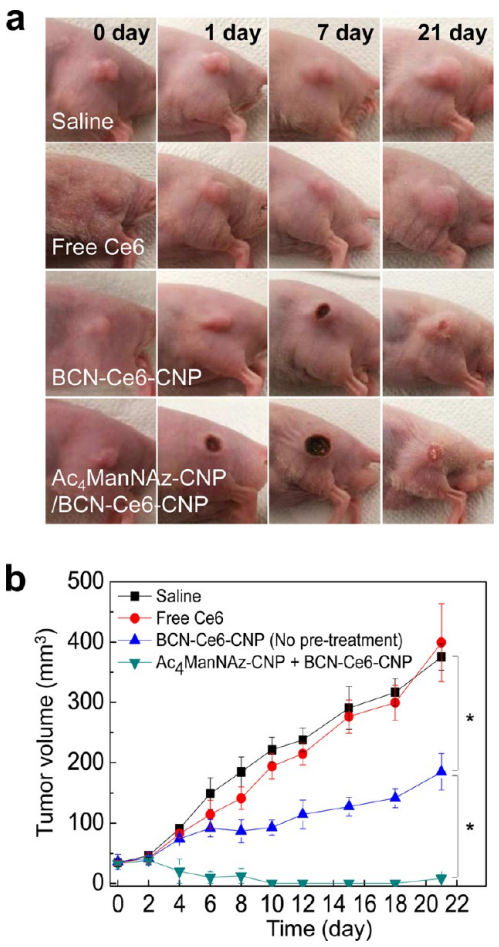

Figure 9. ***In vivo*** **photodynamic therapy with Ac_4ManNAz-CNP and BCN-Ce6-CNP in tumor-bearing mice. (a) Tumor images of mice treated with free Ce6 or nanoparticles and irradiated with a laser. (b) Measured tumor growth for 21 days after photodynamic therapy. Asterisk (*) indicates difference at the $p < 0.01$ significance level ($n = 5$).**

Finally, we evaluated the therapeutic efficacy of our two-step strategy using the same A549 tumor-bearing mice. After laser irradiation, significant bleeding and black scab generation was observed in mice treated with Ac_4ManNAz-CNP and BCN-Ce6-CNP. This is direct evidence of tumor tissue destruction by excessive local generation of cytotoxic singlet oxygen (Figure 9a). Twenty-one days post laser irradiation, the scabs detached and tumor tissue could not grow further in this group (average tumor volume was 8.5 mm^3 after three weeks), indicating successful tumor therapy by our two-step tumor-targeting strategy (Figure 9b). Without pretreatment of Ac_4ManNAz-CNP, the size of the tumor tissue increased slowly to 184.9 mm^3 due to incomplete destruction of the tumor. As expected, free Ce6-treated mice showed explosive tumor growth to 375.5 mm^3, which is similar to the case of saline treatment (399.4 mm^3), since free Ce6 has no tumor-targeting ability. It is interesting that the gap of therapeutic efficacy originated from only 1.8-fold higher accumulation of BCN-Ce6-CNP in tumor tissue in two-step strategy compared to the case without pretreatment. We carefully expect that more CNPs in tumor tissue might bind tumor cells by click chemistry and moved into the cells, not remaining in the extracellular region. Then, they are more effective for therapy even though the whole body distributions were not much different similarly with the cases with biological ligands.[47] Together, these results demonstrate that the enhanced tumor targeting of nanoparticles by our two-step strategy can be applied to drug delivery and significantly increase the therapeutic efficacy *in vivo*.

To generate 'receptor-like' chemical groups on tumor tissue, we used metabolic glycoengineering under *in vivo* conditions. Metabolic glycoengineering is a useful technique that can insert unnatural sugars with functional groups like azide, thiol, or aldehyde into cellular glycans like sialic acid. The Bertozzi group has demonstrated that this technique can occur inside the living body including cell, embryo, zebrafish, and mice, and proposed its various biological applications.[48] Importantly, in this paper, we proved for the first time that metabolic glycoengineering can specifically occur in tumor tissue *in vivo* by intravenous injection. Thus, it is now possible to modify the cell surface in tumor tissue *in vivo* specifically with chemical functional groups through metabolic glycoengineering. We expect that specific functional groups on tumor tissue can enable chemical binding with various materials, including nanoparticles, and it can be useful for imaging, drug delivery, and other biomedical fields.

To apply copper-free click chemistry *in vivo*, we utilized chemical binding between azides and BCN. The second rate constant of these two groups is about 0.14 M^{-1} s^{-1}, which is about 70-fold faster than Staudinger ligation, a similar bioorthogonal chemical reaction suggested in the early 1900s.[48] The reaction rate of BCN to azide groups was enough to control and change the pharmacokinetics of nanoparticles after intravenous injection. Furthermore, many organic chemists have been developing more advanced click molecules with faster reaction rates; therefore, the tumor-targeting efficiency of the strategy introduced here can be further enhanced with better click molecules.[3]

As mentioned previously, the intrinsic limitations of traditional biological binding molecules originate from the limited number of receptors and the heterogeneity of tumor cells. Our 'receptor-like' chemical groups are azide groups composed of only three nitrogen atoms, so they are much smaller than biological receptors. This small size of the azide group allows them to be expressed on cell surface in large quantity and thereby maximizes the capacity of binding with nanoparticles similarly with the case of cyclooctyne.[49] Furthermore, the efficiency of metabolic glycoengineering is proven to be very high in tumor cells, because most tumor cells have abundant sialic acids on their surface as structural components.[22] The high concentration and

tumor-selective expression of azide groups and their highly efficient binding with BCN led to dramatic improvements in therapeutic efficiency in animal data. To focus on the enhancement of the tumor-targeting of nanoparticle by click chemistry, we did not use any biological binding ligands in this study. This was possible due to the high tumor-targeting ability of our CNP *in vivo*. However, the generation of azide groups can be made more specific if we further modify Ac_4ManNAz-CNP with biological ligands similar to those used in the study by Chen group.[34] The addition of biological ligands will enhance the targeting efficacy of nanoparticles at the cellular level.

CONCLUSION

We propose a two-step *in vivo* tumor-targeting strategy for nanoparticles *via* metabolic glycoengineering and click chemistry. First, intravenous injection of Ac_4ManNAz-CNP generates azide groups on tumor tissue by site-specific metabolic glycoengineering. These azide groups enhance the tumor-targeting ability of a second intravenous injection of BCN-Ce6-CNPs by copper-free click chemistry *in vivo*. Thus, a large amount of drugs can be delivered by the second round of drug-containing nanoparticles. Our successful therapeutic results *in vivo* definitively prove the advantage of this strategy. Importantly, this system uses no biological binding molecules, which are traditionally used to enhance the tumor-targeting ability of nanoparticles. Instead, 'receptor-like' chemical groups are generated by the nanoparticle itself, and copper-free click chemistry *in vivo* enhances the tumor-targeting ability of the next nanoparticle injection. Furthermore, the whole procedure is composed of intravenous injections only, allowing it to be applied to tumor therapy even when the location of the tumor tissue is not well-defined. Our strategy significantly demonstrates the usefulness of copper-free click chemistry in nanoparticle delivery and may have great potential for further biomedical applications.

MATERIALS AND METHODS

Materials. Glycol chitosan (M_w = 2.5 × 10^5 kDa; degree of deacetylation = 82.7%) was purchased from Sigma-Aldrich (St. Louis, MO, USA), purified by filtration, and dialyzed against deionized distilled water. 5β-Cholanic acid, chlorin e6 (Ce6), *N*-hydroxysuccinimide (NHS), 1-ethyl-3-(3-dimethylaminopropyl)-carbodiimide hydrochloride (EDC), fluorescein isothiocyanate (FITC), *p*-nitroso-*N*,*N*′-dimethylaniline (RNO), folic acid, ethylenediamine (EDA), and MTT (3-(4,5-dimethylthiazol-2-yl)-2,5-diphenyltetrazolium bromide were purchased from Sigma-Aldrich (St. Louis, MO, USA). The *N*-hydroxysuccinimide ester of Cy5.5 (Cy5.5-NHS) was purchased from GE Healthcare (Piscataway, NJ, USA). Tetraacetylated *N*-azidoacetyl-D-mannosamine (Ac_4ManNAz) was purchased from Invitrogen (Carlsbad, CA, USA). Phosphine-PEG_3-biotin and streptavidin-horseradish peroxidase (streptavidin-HRP) were purchased from Thermo Scientific (Rockford, IL, USA). Dibenzylcyclooctyne-sulforhodamine B (DBCO-sulforhodamine B) and dibenzylcyclooctyne-Cy5 (DBCO-Cy5) were obtained from Click Chemistry Tools (Scottsdale, AZ, USA). Deprotected cyclic RGDyK (Cyclick Arg-Gly-Asp-D-Tyr-Lys, cRGDyK) was purchased from FutureChem (Seoul, Republic of Korea). α-3-(*N*-*t*-Butyloxycarbonylamino)-propyl-ω-(succinimidyloxy carboxy), polyoxyethylene ((t-Boc)-NH_2-PEG-NHS, M_w 2000) was purchased from SUNBRIGHT (NOR Corporation, Tokyo, Japan). Bicyclo[6.1.0]nonyne *N*-hydroxysuccinimide ester II (BCN-NHS) was purchased from Berry & Associates (Dexter, MI, USA). Methanol, dimethylsulfoxide (DMSO), and tetrahydrofuran (THF) were purchased from Merck (Darmstadt, Germany). All chemicals were of analytical grade and used without further purification except glycol chitosan.

Synthesis of Glycol Chitosan Nanoparticle (CNP). Self-assembled glycol chitosan nanoparticle (CNP) was prepared by conjugation of hydrophobic 5β-cholanic acid to the primary amine groups of glycol chitosan polymers. Briefly, to activate carboxylic acid group of 5β-cholanic acid with NHS, 5β-cholanic acid (150 mg, 400 μmol) was dissolved in 60 mL of methanol and mixed with EDC (120 mg, 600 μmol, 1.5 equiv of 5β-cholanic acid) and NHS (72 mg, 600 μmol, 1.5 equiv of 5β-cholanic acid). Then, glycol chitosan (500 mg, 2 μmol) was dissolved in methanol/deionized distilled water mixture (1:1 v/v, 60 mL) and added to the methanol solution containing NHS-activated 5β-cholanic acid. The resulting solution was stirred overnight at room temperature, and then dialyzed for 2 days in deionized distilled water/methanol (1:3 v/v) using a cellulose membrane (MWCO 12−14000, Spectrum Laboratories, Laguna Hills, CA, USA). The solution was further dialyzed for 2 days in deionized distilled water and lyophilized to give glycol chitosan-5β-cholanic acid conjugates. The degree of substitution (DS), defined as the number of 5β-cholanic acid per one glycol chitosan polymer, was determined using a colloidal titration method. The final conjugates had 218 ± 0.4 molecules of 5β-cholanic acids per one glycol chitosan polymer.

Preparation of Ac_4ManNAz-Loaded CNP. Ac_4ManNAz was dissolved in 200 μL of THF and added dropwise into the glycol chitosan-5β-cholanic acid solutions (20 mg/6 mL) in THF/deionized distilled water (1:1 v/v) with sonication. Then, the organic solvent was evaporated by the rotatory evaporator resulting in the deposition of a thin film on the glass vial wall. The film was freeze-dried for 4 h to remove remaining organic solvent and then hydrated and dispersed in deionized distilled water by sonication. The solution was filtered through a 0.45 μm syringe filter membrane (cellulose acetate, Millipore) to remove unloaded Ac_4ManNAz and lyophilized. Then, it was dispersed in deionized distilled water or PBS buffer (pH 7.4) by sonication to produce Ac_4ManNAz-loaded CNPs. The size distribution of Ac_4ManNAz-CNP was measured using a Zetasizer Nano ZS (Malvern Instruments, Worcestershire, U.K.). The samples were dispersed in deionized distilled water (1 mg/mL) and size was measured at 25 °C. The morphological shapes of nanoparticles were directly determined using transmission electron microscopy (TEM) (CM-200, Philips, CA, USA). Freshly prepared Ac_4ManNAz-CNPs (1 mg/mL in deionized distilled water) were dropped onto a 400-mesh copper grid, and stained with 5% (w/v) uranyl acetate solution before imaging. The loading content of Ac_4ManNAz in CNPs was determined using high performance liquid chromatography (HPLC).

To label CNPs with Cy5.5 for tracking by fluorescence, Cy5.5-NHS (2 mg, 1.7 μmol) was dissolved in 500 μL of DMSO and added dropwise to the DMSO solution containing glycol chitosan-5β-cholanic acid conjugate (220 mg/80 mL). The reaction mixture was stirred overnight at room temperature, dialyzed against deionized distilled water using a cellulose membrane (MWCO 12−14000) for 2 days, and lyophilized to give Cy5.5-labeled CNP.

Synthesis of BCN-Ce6-CNP. First, BCN-NHS was chemically conjugated to the glycol chitosan polymers using the similar amide bond formation. Briefly, BCN-NHS (10 mg, 19 μmol) was dissolved in 500 μL of DMSO and added dropwise to the glycol

chitosan polymer (100 mg, 12 mL) in 1:9 (v/v) DMSO/deionized distilled water. The reaction mixture was stirred overnight at room temperature, dialyzed against DMSO and deionized distilled water using a cellulose membrane (MWCO 12−14000) for 2 days, and lyophilized to obtain white powder.

Second, BCN-conjugated glycol chitosan polymer (50 mg, 200 nmol) was dissolved in 1:9 (v/v) DMSO/deionized distilled water (10 mL), and Ce6 (5 mg) was dissolved in DMSO (1 mL). Then, 5.73 mg (30 μmol) of EDC and 3.45 mg (30 μmol) of NHS were added to the solution. It was gently stirred overnight at room temperature, dialyzed for 3 days against DMSO and deionized distilled water to remove free Ce6 molecules, and lyophilized to give a green powder containing BCN-Ce6-GC conjugates. The resulting samples were dispersed in PBS buffer (pH 7.4) by sonication to produce nanosized BCN-Ce6-CNPs. The sizes and morphological shapes of BCN-Ce6-CNPs were similarly measured using a Zetasizer and TEM. The chemical conjugation efficiency of Ce6 was quantified using a UV/vis spectrophotometer Lambda 7 (Perkin-Elmer, CT, USA). The Ce6 concentration was determined by measuring absorbance at 405 nm and referring to a standard curve of free Ce6 concentrations in the same DMSO/deionized distilled water solution.

The chemical structure of BCN-Ce6-CNP was characterized with ^{1}H NMR. ^{1}H NMR spectra were obtained at 400 MHz, using DMSO-*d* as a solvent. ^{1}H NMR peaks are as follows: 0.97−0.99 (H of CH_3 from Ce6, 3H), 1.04−1.06 (H of CH_3 from Ce6, 3H), 3.10−3.12 (H of CH_2−CO from Ce6, 2H), 4.06−4.08 (H of CH_2−CO from BCN, 8H). As shown in Figure S1, peaks of Ce6 at 0.97−1.06 and 3.10−3.12 ppm, glycol chitosan peaks at 2.71−3.85 ppm and BCN peaks at 4.06−4.08 ppm could be observed in NMR spectra.

Singlet Oxygen Generation from BCN-Ce6-CNP. The generation of singlet oxygen from Ce6 was quantitatively observed using RNO as a singlet oxygen indicator. To measure the singlet oxygen generation, free Ce6 (100 μg/mL), and BCN-Ce6-CNPs (100 μg/mL of Ce6) in 200 μL of 1:1 (v/v) DMSO/deionized distilled water were added to 3.8 mL of 1:1 (v/v) DMSO/deionized distilled water containing 5.88 mg of L-histidine and 0.377 μg of RNO. Then each solution was irradiated using 671 nm He−Ne laser (DPSS 671 nm Red Laser, i-Nexus, Inc.). The absorbance of RNO at 405 nm was measured using a UV/vis spectrophotometer as a function of time.

Cell Culture. A549 (Human lung adenocarcinoma) cells, human nasopharyngeal carcinoma cells (KB), human glioblastoma cells (U87MG), human mammary carcinoma cells (MCF-7), and human breast adenocarcinoma cells (MDA-MB-436 and MDA-MB-468) were purchased from ATCC (Manassas, VA, USA), maintained in RPMI1640 (Welgene, Daegu, Korea) containing 10% fetal bovine serum (FBS; Welgene, Daegu, Korea), 100 μg/mL streptomycin and 100 U/mL penicillin (Welgene, Daegu, Korea) in a humidified 5% CO_2 atmosphere at 37 °C.

Cellular Imaging To Determine the Generated Azide Groups. A549 cells were seeded onto 35 mm glass-bottom dishes at a density of 3×10^4 cells in 2 mL of growth media with Ac_4ManNAz (50 μM) or Ac_4ManNAz-loaded CNPs (50 μM Ac_4ManNAz). After incubation for three days, the cells were washed twice with DPBS (pH 7.4), and incubated with DBCO-sulforhodamine B (200 μM, final concentration) for 1 h at 37 °C. Then, cells were rinsed with DPBS (pH 7.4) and fixed with formaldehyde−glutaraldehyde combined fixative for 10 min at room temperature. After fixation, the cells were washed twice with DPBS (pH 7.4), and stained with DAPI (Invitrogen, Carlsbad, CA, USA) to label nuclei. All cellular images were obtained using a FluoView FV1000 confocal laser scanning microscope (Olympus, Tokyo, Japan) equipped with a 405 diode (405 nm), HeNe-Green (543 nm), and HeNe-Red (633 nm) lasers. Time-dependent duration of azide groups was also observed by further incubation of cells after incubation with Ac_4ManNAz or Ac_4ManNAz-CNP. After 3 days incubation of Ac_4ManNAz or Ac_4ManNAz-CNP, the cells were further incubated for 1−40 h and treated with DBCO-sulforhodamine B. Fixation and imaging process were done in the same condition.

Western Blot Analysis of Cells. A549 cells were seeded onto 100 × 20 mm cell culture plates at a density of 2×10^6 cells per plate in 12 mL of media with Ac_4ManNAz (50 μM) or Ac_4ManNAz-loaded CNPs (50 μM Ac_4ManNAz). After incubation for three days, the cells were washed twice with DPBS (pH 7.4) and harvested from the plates with a cell scraper. They were pelleted by centrifugation at 1500 rpm for 5 min, and the cell pellets were resuspended in 500 μL of lysis buffer (1% SDS, 100 mM Tris·HCl, pH 7.4) containing protease inhibitor cocktail (Complete, EDTA-free, Roche, NSW, Australia). After 30 min incubation at 4 °C, the insoluble debris was removed by centrifugation for 10 min at 3000 rpm. Final soluble protein concentrations were adjusted by bicinchoninic acid (BCA) protein assay (Pierce, Rockford, IL, USA) to be 5 mg/mL. Then, 20 μL of the lysate was incubated with phosphine-PEG_3-biotin (2 μL, 5 mM in DPBS) (Pierce, Rockford, IL, USA) for 6 h at 37 °C. Loading buffer was added to each sample, and samples were loaded onto 10% SPS-PAGE gel after heating at 95 °C. Proteins were transferred to Hybond P membrane (Amercham, St. Albans, U.K.), and the membrane was blocked with 5% bovine serum albumin (BSA) in TBST (50 mM Tris·HCl, 150 mM NaCl, 0.1% Tween20, pH 7.4) for 2 h. Then, the membrane was incubated with streptavidin-HRP (diluted 1:2000 in TBST) (Pierce, Rockford, IL, USA) overnight at 4 °C. The membrane was rinsed three times with TBST and developed by using ECL Western Blotting Substrate (Pierce, Rockford, IL, USA).

Cellular Imaging To Show the Binding of BCN-Ce6-CNP. Only for the cellular imaging, BCN-Ce6-CNPs were labeled with 0.1 wt % FITC in DMSO and purified again. After FITC labeling, the physicochemical properties such as particle size and morphological shape were not significantly changed compared to unlabeled BCN-Ce6-CNPs.

A549 cells were seeded onto 35 mm glass-bottom dishes at a density of 3×10^4 cells in 2 mL of media with Ac_4ManNAz (50 μM) or Ac_4ManNAz-loaded CNPs (50 μM Ac_4ManNAz). After incubation for three days, the cells were washed twice with DPBS (pH 7.4) and incubated with FITC-labeled BCN-Ce6-CNPs at a concentration of 100 μg/mL for 1 h at 37 °C in 2 mL serum-free media. After that, the cells were rinsed twice with DPBS (pH 7.4), fixed with formaldehyde−glutaraldehyde combined fixative for 10 min at room temperature, and stained with DAPI to label nuclei.

Flow Cytometry Analysis. A549 cells were pretreated with Ac_4ManNAz (50 μM) or Ac_4ManNAz-loaded CNPs and treated with FITC-labeled BCN-Ce6-CNPs, as mentioned above. Then, cells were lifted with DPBS containing 2% FBS (FACS buffer) and washed twice in FACS buffer. Twenty thousand cells per sample were analyzed by flow cytometry (BD FACSVerse, BD Biosciences, San Jose, CA, USA) and subsequent data analysis was performed using FlowJo software.

Time-Lapse Cellular Imaging. For time-lapse imaging, A549 cells were seeded onto 35 mm glass-bottom dishes at a density of 3×10^4 cells in 2 mL of media with Ac_4ManNAz-loaded CNPs (50 μM Ac_4ManNAz). After incubation for three days, the cells were washed twice with DPBS (pH 7.4) and incubated with FITC-labeled BCN-Ce6-CNPs at a concentration of 100 μg/mL for 1 h at 37 °C in 2 mL serum-free media. After that, the cells were washed twice with DPBS (pH 7.4) and replaced with fresh growth media. The cells were fixed at different time points from 0 to 24 h and observed by microscopy.

Imaging of the Bindings of Biological Ligands or Click Molecules to Tumor Cells. To prepare folate-PEG-Cy5.5, folic acid (10 mg) was first added into 60 mL of ethylenediamine (EDA) and stirred in the dark at room temperature for 3 h. After precipitation in acetone twice, the precipitate was dissolved in water and filtrated to remove the insoluble substance. Then, this folate-EDA (20 mg, 24 μmol) was incubated with (t-Boc)-NH_2-PEG-NHS (M_w 2000) in 2.5 mL of DMSO for 2 h, and treated by TFA for deprotection of t-Boc. Next, this folate-PEG conjugates (10 mg; 4 μmol) was incubated with Cy5.5-NHS (10 μmol) in 500 μL of phosphate buffer (10 mM, pH 7.4) for 2 h in the dark at room temperature. The final product, folate-PEG-Cy5.5 conjugate, was purified by HPLC. cRGD-PEG-Cy5.5 was prepared by similar amide coupling of c(RGDyK) with (t-Boc)-protected PEG-NHS (M_w 2000), followed by TFA cleavage. Then, this cRGD-PEG conjugate (8 mg; 2 μmol) was incubated with Cy5.5-NHS (10 μmol) in 500 μL of phosphate buffer (10 mM, pH 7.4) for 2 h in the dark at room temperature. Final product was also

purified by HPLC. Cetuximab-Cy5.5 was prepared by the reaction between anti-EGFR monoclonal antibody, Cetuximab (3.3 nmol) and Cy5.5-NHS (40 nmol) in phosphate buffer (0.1 M, pH 8.5). After a 2 h reaction, the mixture was purified with PD-10 column to remove unbound Cy5.5

All cells were seeded onto 35 mm glass-bottom dishes at a density of 3×10^4 cells in 2 mL of growth media with no sugar or Ac_4ManNAz-CNPs (50 μM Ac_4ManNAz). After incubation for three days, the cells were washed twice with DPBS (pH 7.4), and incubated with DBCO-Cy5 (20 μM, final concentration) for 30 min at 37 °C for cellular imaging. The same method was used for the case of KB, U87MG, MCF-7, MDA-MB-468, and MDA-MB-436 cells.

For the comparative study using traditional biological binding molecules, all cells were seeded onto 35 mm glass-bottom dishes at a density of 3×10^4 cells in 2 mL of growth media and grown to reach 60−80% confluence. The cells were washed twice with DPBS (pH 7.4), and incubated with Folate-PEG-Cy5.5 (0.2 μM, final concentration), RGD-PEG-Cy5.5 (0.2 μM, final concentration), or Cetuximab-Cy5.5 (0.1 μM, final concentration) for 30 min at 37 °C for cellular imaging.

Cell Viability Assay. To measure cell viability, A549 cells were seeded on 96-well plates (5×10^3 cells/well) and incubated for one day. To test the cytotoxicity of Ac_4ManNAz-loaded CNPs, they were treated with Ac_4ManNAz (50 μM) or Ac_4ManNAz-CNPs (50 μM Ac_4ManNAz). After incubation for three days, the cells were washed twice with DPBS (pH 7.4) and 25 μL of MTT in serum-free RPMI1640 media (0.5 mg/mL) was added to each well. After further incubation for 4 h at 37 °C, the media was removed and cells were dissolved in 200 μL of DMSO. Then, the absorbance of each well was measured at 570 nm using a microplate reader (VERSAmaxTM, Molecular Devices Corp., Sunnyvale, CA).

To measure cell viability before laser irradiation, the cells were incubated with free Ce6 or BCN-Ce6-CNPs (0−20 μg/mL of Ce6) at 37 °C. After 1 h of incubation, cell viability was determined by MTT assay similarly. To measure cell viability after laser irradiation, A549 cells were seeded on 96-well plates (5×10^3 cells/well) and treated with Ac_4ManNAz (50 μM) or Ac_4ManNAz-loaded CNPs (50 μM Ac_4ManNAz). After incubation for one day, the cells were washed twice with DPBS (pH 7.4) and incubated with BCN-Ce6-CNPs (2.5 μg/mL of Ce6) for 1 h at 37 °C. Then, the cells were washed twice with serum-free media and irradiated with a 671 nm He−Ne laser (100 mW/cm^2) for 0−4 min onto the 96-well plates. After 6 h of incubation, cell viability was determined by MTT assay similarly.

***In Vivo* Imaging.** All experiments with live animals were performed in compliance with the relevant laws and institutional guidelines of Korea Institute of Science and Technology (KIST), and institutional committees approved the experiments. A549 tumor cells (1.0×10^7 cells) were injected subcutaneously on flanks of 4-week-old male athymic nude mice (20 g, Institute of Medical Science, Tokyo, Japan). When the tumor reached about 100 mm^2, Ac_4ManNAz (40 mg/kg) or Ac_4ManNAz-CNPs (40 mg Ac_4ManNAz/kg) were administered into A549 tumor-bearing mice by intravenous injection once a day for 4 days. Bare CNPs and Ac_4ManNAz-CNPs were labeled with Cy5.5 for *in vivo* monitoring. Free Ce6 (2.5 mg/kg) or BCN-Ce6-CNPs (2.5 mg/kg of Ce6) were injected into the tail vein of the A549 tumor-bearing mice, and their biodistribution and tumor accumulation was observed based on the intrinsic fluorescence of Ce6 using the eXplore Optix system (ART Advanced Research Technologies Inc., Montreal, Canada). Laser power, exposure time and count time settings were optimized at 5 μW and 0.3 s per point. The NIRF emission at 700 nm was collected and detected with a fast photomultiplier tube (Hamamatsu, Japan) and a time-correlated single photon counting system (Becker and Hickl GmbH, Berlin, Germany). All data were calculated using the region of interest (ROI) function of the Analysis Workstation software (ART Advanced Research Technologies Inc., Montreal, Canada), and values were presented as means ± SE for groups ($n = 3$). For the comparative analysis of quenched azide groups on tumor tissue, A549 tumors were induced into nude mice on both sides of flank, and Ac_4ManNAz-loaded CNPs (40 mg Ac_4ManNAz/kg) were injected intravenously. Then, 20 μL of TCEP solution (10 mM) was injected into the left tumors by intratumoral injection for chemical quenching of generated azide groups. After 1 h, BCN-Ce6-CNPs were injected intravenously and analyzed by same the imaging method.

***Ex Vivo* Imaging.** The major organs and tumors were dissected from mice 48 h postinjection of free Ce6 or BCN-Ce6-CNPs. Fluorescence images was obtained with a 12-bit CCD (Kodak Image Station 4000 MM, New Haven, CT, USA) equipped with a special C-mount lens and a near-infrared emission filter (600−700 nm; Omega Optical, Brattleboro, VT, USA). The nanoparticle amount in tissues was quantified by measuring the fluorescence signal intensity at the ROI using KODAK molecular imaging software. All values were presented as means ± SE for groups ($n = 3$).

For histological evaluation, dissected tumors were frozen in optimum cutting temperature (OCT) tissue compound (Sakura, Tokyo, Japan) on dry ice and sectioned into 6 μm slices. Fluorescence of tumor tissue sections was viewed by IX81-ZDC focus drift compensating microscope (Olympus, Tokyo, Japan).

Measurement of the Concentration of CNPs in Blood. To quantify the concentration of nanoparticles in the blood, 1 mL of blood samples (Cy5.5, Cy5.5-labeled Ac4ManNAz-CNPs, Ce6, and BCN-Ce6-CNPs ($n = 5$) was drawn from mice at different time points and centrifuged at 1000 rpm for 20 min. NIRF images and intensity graph of the supernatant fractions were evaluated using a 12-bit CCD camera. The intensities were recorded as total photons per second per centimeter squared per steradian [photons(s·cm^2·sr)].

Western Blot Analysis of Tissues. The preparation of A549 tumor-bearing mice models and intravenous injection of Ac_4ManNAz (40 mg/kg) or Ac_4ManNAz-CNPs (40 mg Ac_4ManNAz/kg) were performed by the same method. One day after the last injection of Ac_4ManNAz or Ac_4ManNAz-CNPs, the major organs and tumors were dissected and transferred into 1 mL of lysis buffer (1% SDS, 100 mM Tris·HCl, pH 7.4) containing protease inhibitor cocktail (Complete, EDTA-free, Roche, NSW, Australia) and homogenized. The lysates were incubated at 4 °C for 30 min, and insoluble debris was removed by centrifugation for 10 min at 3000 rpm. Total soluble protein concentrations were measured using BCA protein assay kit. Then, Western blot analysis was performed with phosphine-PEG_3-biotin by the same method as the cell lysate analysis.

Immunohistochemical Analysis. The dissected major organs and tumor tissues were retrieved from A549 tumor-bearing mice, fixed in 4% (v/v) buffered formalin solution for 30 min at room temperature, dehydrated with a graded ethanol series, and embedded in paraffin. Immunohistochemical staining was performed using phosphine-PEG_3-biotin and streptavidin-HRP according to the standard methods. Paraffin slices were observed with a light microscope (BX51, Olympus, Tokyo, Japan). Images were photographed on a digital camera photomicroscope (DP71, Olympus, Tokyo, Japan).

***In Vivo* Photodynamic Therapy (PDT).** The A549 tumor-bearing mice models were prepared similarly to the imaging studies. When tumors grew to 35 ± 10 mm^3 in volume, saline or Ac_4ManNAz-CNPs (40 mg Ac_4ManNAz/kg) were administered into A549 tumor-bearing mice by intravenous injection once a day for 4 days. After that, saline, free Ce6 (2.5 mg/kg), or BCN-Ce6-CNPs (2.5 mg/kg of Ce6) were injected into the mice *via* tail vein ($n = 4$ per each group). At 6 and 48 h after injection of Ce6 or BCN-Ce6-CNPs, tumor-tissues were irradiated by 671 nm He−Ne laser (100mW/cm^2) for 30 min each. The therapeutic results of each group were evaluated by measuring the tumor volumes for 21 days.

Statistics. In this study, the differences between experimental and control groups were analyzed using one-way ANOVA and considered statistically significant (marked with an asterisk (*) in figure) if $p < 0.01$, respectively.

Conflict of Interest: The authors declare no competing financial interest.

Acknowledgment. This study was funded by the Global Research Laboratory Project (NRF-2013K1A1A2032346 & NRF-2013K1A1A2A02050115), the Fusion Technology Project

(2009-0081876), and the Intramural Research Program (Theragnosis) of KIST.

Supporting Information Available: Synthetic scheme, additional images, and graphs. This information is available free of charge *via* the Internet at http://pubs.acs.org.

REFERENCES AND NOTES

1. Kolb, H. C.; Finn, M. G.; Sharpless, K. B. Click Chemistry: Diverse Chemical Function from a Few Good Reactions. *Angew. Chem., Int. Ed.* **2001**, *40*, 2004–2021.
2. Boyce, M.; Bertozzi, C. R. Bringing Chemistry to Life. *Nat. Methods* **2011**, *8*, 638–642.
3. Bertozzi, C. R. A Decade of Bioorthogonal Chemistry. *Acc. Chem. Res.* **2011**, *44*, 651–653.
4. Jewett, J. C.; Bertozzi, C. R. Cu-Free Click Cycloaddition Reactions in Chemical Biology. *Chem. Soc. Rev.* **2010**, *39*, 1272–1279.
5. Ngo, J. T.; Champion, J. A.; Mahdavi, A.; Tanrikulu, I. C.; Beatty, K. E.; Connor, R. E.; Yoo, T. H.; Dieterich, D. C.; Schuman, E. M.; Tirrell, D. A. Cell-Selective Metabolic Labeling of Proteins. *Nat. Chem. Biol.* **2009**, *5*, 715–717.
6. Shelbourne, M.; Chen, X.; Brown, T.; El-Sagheer, A. H. Fast Copper-Free Click DNA Ligation by the Ring-Strain Promoted Alkyne-Azide Cycloaddition Reaction. *Chem. Commun.* **2011**, *47*, 6257–6259.
7. Bertozzi, C. R.; Kiessling, L. L. Chemical Glycobiology. *Science* **2001**, *291*, 2357–2364.
8. Boyce, M.; Carrico, I. S.; Ganguli, A. S.; Yu, S.-H.; Hangauer, M. J.; Hubbard, S. C.; Kohler, J. J.; Bertozzi, C. R. Metabolic Cross-Talk Allows Labeling of O-Linked β-N-Acetylglucosamine-Modified Proteins *via* the N-Acetylgalactosamine Salvage Pathway. *Proc. Natl. Acad. Sci. U. S. A.* **2011**, *108*, 3141–3146.
9. Gartner, Z. J.; Bertozzi, C. R. Programmed Assembly of 3-Dimensional Microtissues with Defined Cellular Connectivity. *Proc. Natl. Acad. Sci. U. S. A.* **2009**, *106*, 4606–4610.
10. Laughlin, S. T.; Baskin, J. M.; Amacher, S. L.; Bertozzi, C. R. *In Vivo* Imaging of Membrane-Associated Glycans in Developing Zebrafish. *Science* **2008**, *320*, 664–667.
11. Colombo, M.; Sommaruga, S.; Mazzucchelli, S.; Polito, L.; Verderio, P.; Galeffi, P.; Corsi, F.; Tortora, P.; Prosperi, D. Site-Specific Conjugation of ScFvs Antibodies to Nanoparticles by Bioorthogonal Strain-Promoted Alkyne−Nitrone Cycloaddition. *Angew. Chem., Int. Ed.* **2012**, *51*, 496–499.
12. Devaraj, N. K.; Weissleder, R. Biomedical Applications of Tetrazine Cycloadditions. *Acc. Chem. Res.* **2011**, *44*, 816–827.
13. Cheng, Z.; Al Zaki, A.; Hui, J. Z.; Muzykantov, V. R.; Tsourkas, A. Multifunctional Nanoparticles: Cost *versus* Benefit of Adding Targeting and Imaging Capabilities. *Science* **2012**, *338*, 903–910.
14. Lee, D.-E.; Koo, H.; Sun, I.-C.; Ryu, J. H.; Kim, K.; Kwon, I. C. Multifunctional Nanoparticles for Multimodal Imaging and Theragnosis. *Chem. Soc. Rev.* **2012**, *41*, 2656–2672.
15. Koo, H.; Huh, M. S.; Ryu, J. H.; Lee, D.-E.; Sun, I.-C.; Choi, K.; Kim, K.; Kwon, I. C. Nanoprobes for Biomedical Imaging in Living Systems. *Nano Today* **2011**, *6*, 204–220.
16. Liu, T. W.; MacDonald, T. D.; Jin, C. S.; Gold, J. M.; Bristow, R. G.; Wilson, B. C.; Zheng, G. Inherently Multimodal Nanoparticle-Driven Tracking and Real-Time Delineation of Orthotopic Prostate Tumors and Micrometastases. *ACS Nano* **2013**, *7*, 4221–4232.
17. Maeda, H.; Wu, J.; Sawa, T.; Matsumura, Y.; Hori, K. Tumor Vascular Permeability and the EPR Effect in Macromolecular Therapeutics: a Review. *J. Controlled Release* **2000**, *65*, 271–284.
18. Koo, H.; Huh, M. S.; Sun, I.-C.; Yuk, S. H.; Choi, K.; Kim, K.; Kwon, I. C. *In Vivo* Targeted Delivery of Nanoparticles for Theranosis. *Acc. Chem. Res.* **2011**, *44*, 1018–1028.
19. Bae, Y. H.; Park, K. Targeted Drug Delivery to Tumors: Myths, Reality and Possibility. *J. Controlled Release* **2011**, *153*, 198–205.
20. Park, J. W.; Hong, K.; Kirpotin, D. B.; Colbern, G.; Shalaby, R.; Baselga, J.; Shao, Y.; Nielsen, U. B.; Marks, J. D.; Moore, D.; *et al.* Anti-HER2 Immunoliposomes. *Clin. Cancer. Res.* **2002**, *8*, 1172–1181.
21. Denison, T. A.; Bae, Y. H. Tumor Heterogeneity and Its Implication for Drug Delivery. *J. Controlled Release* **2012**, *164*, 187–191.
22. Koo, H.; Lee, S.; Na, J. H.; Kim, S. H.; Hahn, S. K.; Choi, K.; Kwon, I. C.; Jeong, S. Y.; Kim, K. Bioorthogonal Copper-Free Click Chemistry *in Vivo* for Tumor-Targeted Delivery of Nanoparticles. *Angew. Chem., Int. Ed.* **2012**, *51*, 11836–11840.
23. Saxon, E.; Bertozzi, C. R. Cell Surface Engineering by a Modified Staudinger Reaction. *Science* **2000**, *287*, 2007–2010.
24. Lin, L.; Tian, X.; Hong, S.; Dai, P.; You, Q.; Wang, R.; Feng, L.; Xie, C.; Tian, Z.-Q.; Chen, X.; Bioorthogonal Raman, A. Reporter Strategy for SERS Detection of Glycans on Live Cells. *Angew. Chem., Int. Ed.* **2013**, *52*, 7266–7271.
25. Na, J. H.; Koo, H.; Lee, S.; Min, K. H.; Park, K.; Yoo, H.; Lee, S. H.; Park, J. H.; Kwon, I. C.; Jeong, S. Y.; *et al.* Real-Time and Non-Invasive Optical Imaging of Tumor-Targeting Glycol Chitosan Nanoparticles in Various Tumor Models. *Biomaterials* **2011**, *32*, 5252–5261.
26. Na, J. H.; Lee, S.-Y.; Lee, S.; Koo, H.; Min, K. H.; Jeong, S. Y.; Yuk, S. H.; Kim, K.; Kwon, I. C. Effect of the Stability and Deformability of Self-Assembled Glycol Chitosan Nanoparticles on Tumor-Targeting Efficiency. *J. Controlled Release* **2012**, *163*, 2–9.
27. Nam, H. Y.; Kwon, S. M.; Chung, H.; Lee, S.-Y.; Kwon, S.-H.; Jeon, H.; Kim, Y.; Park, J. H.; Kim, J.; Her, S.; *et al.* Cellular Uptake Mechanism and Intracellular Fate of Hydrophobically Modified Glycol Chitosan Nanoparticles. *J. Controlled Release* **2009**, *135*, 259–267.
28. Green, D. J.; Pagel, J. M.; Pantelias, A.; Hedin, N.; Lin, Y.; Wilbur, D. S.; Gopal, A.; Hamlin, D. K.; Press, O. W. Pretargeted Radioimmunotherapy for B-Cell Lymphomas. *Clin. Cancer. Res.* **2007**, *13*, 5598s–5603s.
29. Rossin, R.; Renart Verkerk, P.; van den Bosch, S. M.; Vulders, R. C. M.; Verel, I.; Lub, J.; Robillard, M. S. *In Vivo* Chemistry for Pretargeted Tumor Imaging in Live Mice. *Angew. Chem., Int. Ed.* **2010**, *49*, 3375–3378.
30. Kim, K.; Kim, J. H.; Park, H.; Kim, Y.-S.; Park, K.; Nam, H.; Lee, S.; Park, J. H.; Park, R.-W.; Kim, I.-S.; *et al.* Tumor-Homing Multifunctional Nanoparticles for Cancer Theragnosis: Simultaneous Diagnosis, Drug Delivery, and Therapeutic Monitoring. *J. Controlled Release* **2010**, *146*, 219–227.
31. Koo, H.; Moon, H.; Han, H.; Na, J. H.; Huh, M. S.; Park, J. H.; Woo, S. J.; Park, K. H.; Kwon, I. C.; Kim, K.; *et al.* The Movement of Self-Assembled Amphiphilic Polymeric Nanoparticles in the Vitreous and Retina after Intravitreal Injection. *Biomaterials* **2012**, *33*, 3485–3493.
32. Laughlin, S. T.; Bertozzi, C. R. Metabolic Labeling of Glycans with Azido Sugars and Subsequent Glycan-Profiling and Visualization *via* Staudinger Ligation. *Nat. Protoc.* **2007**, *2*, 2930–2944.
33. Matsumoto, A.; Cabral, H.; Sato, N.; Kataoka, K.; Miyahara, Y. Assessment of Tumor Metastasis by the Direct Determination of Cell-Membrane Sialic Acid Expression. *Angew. Chem., Int. Ed.* **2010**, *49*, 5494–5497.
34. Xie, R.; Hong, S.; Feng, L.; Rong, J.; Chen, X. Cell-Selective Metabolic Glycan Labeling Based on Ligand-Targeted Liposomes. *J. Am. Chem. Soc.* **2012**, *134*, 9914–9917.
35. Debets, M. F.; van Berkel, S. S.; Dommerholt, J.; Dirks, A. J.; Rutjes, F. P. J. T.; van Delft, F. L. Bioconjugation with Strained Alkenes and Alkynes. *Acc. Chem. Res.* **2011**, *44*, 805–815.
36. Lee, S. J.; Koo, H.; Lee, D.-E.; Min, S.; Lee, S.; Chen, X.; Choi, Y.; Leary, J. F.; Park, K.; Jeong, S. Y.; *et al.* Tumor-Homing Photosensitizer-Conjugated Glycol Chitosan Nanoparticles for Synchronous Photodynamic Imaging and Therapy Based on Cellular On/Off System. *Biomaterials* **2011**, *32*, 4021–4029.
37. Torchilin, V. Tumor Delivery of Macromolecular Drugs Based on the EPR Effect. *Adv. Drug Delivery Rev.* **2011**, *63*, 131–135.
38. Tian, B.; Wang, C.; Zhang, S.; Feng, L.; Liu, Z. Photothermally Enhanced Photodynamic Therapy Delivered by Nano-Graphene Oxide. *ACS Nano* **2011**, *5*, 7000–7009.

39. Sampathkumar, S.-G.; Li, A. V.; Yarema, K. J. Synthesis of Non-Natural ManNAc Analogs for the Expression of Thiols on Cell-Surface Sialic Acids. *Nat. Protoc.* **2006**, *1*, 2377–2385.
40. Ning, X.; Guo, J.; Wolfert, M. A.; Boons, G.-J. Visualizing Metabolically Labeled Glycoconjugates of Living Cells by Copper-Free and Fast Huisgen Cycloadditions. *Angew. Chem., Int. Ed.* **2008**, *47*, 2253–2255.
41. Neves, A. A.; Stöckmann, H.; Harmston, R. R.; Pryor, H. J.; Alam, I. S.; Ireland-Zecchini, H.; Lewis, D. Y.; Lyons, S. K.; Leeper, F. J.; Brindle, K. M. Imaging Sialylated Tumor Cell Glycans *in Vivo*. *FASEB J.* **2011**, *25*, 2528–2537.
42. Park, J. H.; Kwon, S.; Lee, M.; Chung, H.; Kim, J.-H.; Kim, Y.-S.; Park, R.-W.; Kim, I.-S.; Bong Seo, S.; Kwon, I. C.; *et al.* Self-Assembled Nanoparticles Based on Glycol Chitosan Bearing Hydrophobic Moieties as Carriers for Doxorubicin: *In Vivo* Biodistribution and Anti-Tumor Activity. *Biomaterials* **2006**, *27*, 119–126.
43. Koo, H.; Min, K. H.; Lee, S. C.; Park, J. H.; Park, K.; Jeong, S. Y.; Choi, K.; Kwon, I. C.; Kim, K. Enhanced Drug-Loading and Therapeutic Efficacy of Hydrotropic Oligomer-Conjugated Glycol Chitosan Nanoparticles for Tumor-Targeted Paclitaxel Delivery. *J. Controlled Release* **2013**, *172*, 823–831.
44. Min, K. H.; Park, K.; Kim, Y.-S.; Bae, S. M.; Lee, S.; Jo, H. G.; Park, R.-W.; Kim, I.-S.; Jeong, S. Y.; Kim, K.; *et al.* Hydrophobically Modified Glycol Chitosan Nanoparticles-Encapsulated Camptothecin Enhance the Drug Stability and Tumor Targeting in Cancer Therapy. *J. Controlled Release* **2008**, *127*, 208–218.
45. Kim, J.-H.; Kim, Y.-S.; Park, K.; Lee, S.; Nam, H. Y.; Min, K. H.; Jo, H. G.; Park, J. H.; Choi, K.; Jeong, S. Y.; *et al.* Antitumor Efficacy of Cisplatin-Loaded Glycol Chitosan Nanoparticles in Tumor-Bearing Mice. *J. Controlled Release* **2008**, *127*, 41–49.
46. Choi, K. Y.; Yoon, H. Y.; Kim, J.-H.; Bae, S. M.; Park, R.-W.; Kang, Y. M.; Kim, I.-S.; Kwon, I. C.; Choi, K.; Jeong, S. Y.; *et al.* Smart Nanocarrier Based on PEGylated Hyaluronic Acid for Cancer Therapy. *ACS Nano* **2011**, *5*, 8591–8599.
47. Bartlett, D. W.; Su, H.; Hildebrandt, I. J.; Weber, W. A.; Davis, M. E. Impact of Tumor-specific Targeting on the Biodistribution and Efficacy of siRNA Nanoparticles Measured by Multimodality *in Vivo* Imaging. *Proc. Natl. Acad. Sci. U. S. A.* **2007**, *104*, 15549–15554.
48. Sletten, E. M.; Bertozzi, C. R. From Mechanism to Mouse: A Tale of Two Bioorthogonal Reactions. *Acc. Chem. Res.* **2011**, *44*, 666–676.
49. Haun, J. B.; Devaraj, N. K.; Hilderbrand, S. A.; Lee, H.; Weissleder, R. Bioorthogonal Chemistry Amplifies Nanoparticle Binding and Enhances the Sensitivity of Cell Detection. *Nat. Nanotechnol.* **2010**, *5*, 660–665.